JOURNAL OF VIROLOGY, Dec. 2010, p. 12226–12235 Vol. 84, No. 23
0022-538X/10/$12.00 doi:10.1128/JVI.00994-10

Calcium Flux between the Endoplasmic Reticulum and Mitochondrion Contributes to Poliovirus-Induced Apoptosis[▽]

Cynthia Brisac,[1,2,3] François Téoulé,[1,2] Arnaud Autret,[1,2]† Isabelle Pelletier,[1,2] Florence Colbère-Garapin,[1,2] Catherine Brenner,[3,4] Christophe Lemaire,[3,4] and Bruno Blondel[1,2]*

Institut Pasteur, Unité de Biologie des Virus Entériques, 25 rue du Dr Roux, 75015 Paris, France[1]; INSERM U994, Paris, France[2]; Université Versailles Saint-Quentin, Versailles, France[3]; and INSERM U769, Signalisation et Physiopathologie Cardiaque, Châtenay Malabry, France[4]

Received 7 May 2010/Accepted 8 September 2010

We show that poliovirus (PV) infection induces an increase in cytosolic calcium (Ca^{2+}) concentration in neuroblastoma IMR5 cells, at least partly through Ca^{2+} release from the endoplasmic reticulum lumen via the inositol 1,4,5-triphosphate receptor (IP_3R) and ryanodine receptor (RyR) channels. This leads to Ca^{2+} accumulation in mitochondria through the mitochondrial Ca^{2+} uniporter and the voltage-dependent anion channel (VDAC). This increase in mitochondrial Ca^{2+} concentration in PV-infected cells leads to mitochondrial dysfunction and apoptosis.

Poliovirus (PV), the prototype member of the *Picornaviridae* family, is the etiological agent of paralytic poliomyelitis (26, 27). This acute human disease of the central nervous system results from the destruction of motor neurons associated with PV replication. In PV-infected mice, motor neurons die through apoptosis (16). However, the mechanisms involved are poorly understood (5).

Apoptosis is an active cell death process triggered by various stimuli, including viral infections (18). This process leads to DNA fragmentation and is triggered by two main pathways (22): (i) the extrinsic pathway, mediated by the activation of cell surface death receptors such as Fas/CD95, and (ii) the intrinsic pathway, characterized notably by mitochondrial membrane permeabilization (MMP). In many models, this process implies a loss of mitochondrial transmembrane potential ($\Delta\psi_m$) and the release of proapoptotic molecules, including cytochrome *c*, from the mitochondrial intermembrane space into the cytosol. The apoptotic program initiated by PV infection has been shown to involve mitochondrial dysfunction in several cell lines (2–4, 17).

The intrinsic pathway also can originate from the endoplasmic reticulum (ER) (30). The ER participates in protein synthesis and folding, cellular responses to stress, and intracellular calcium (Ca^{2+}) homeostasis. Nevertheless, under stress conditions, it may induce apoptosis via several different mechanisms, one of which involves ER cross-talk with mitochondria, mediated by Ca^{2+} release from ER stores through the inositol 1,4,5-triphosphate receptor (IP_3R) and ryanodine receptor (RyR) channels (7, 12, 15). Several recent studies have identified Ca^{2+} signaling as a key cellular target for viral infection (for a review, see reference 8). Upon PV infection, cells display an increase in cytosolic Ca^{2+} concentration (20). Phospholipase C also is activated, leading to an increase in IP_3 concentration in PV-infected cells (19), potentially accounting for the observed increase in cytosolic Ca^{2+} concentration. However, the role of Ca^{2+} efflux from the ER in PV-induced apoptosis has yet to be studied.

Here, we postulated that an increase in cytosolic Ca^{2+} following PV infection can have an impact on cell fate and investigated the cellular response in terms of mitochondrial function and apoptosis in neuroblastoma IMR5 cells.

MATERIALS AND METHODS

Chemicals and antibodies. Thapsigargin (TG) (T9033), 2-aminoethoxydiphenyl borate (2-APB) (D9754), 4,4′-diisothiocyanatostilbene-2,2′-disulfonic acid (DIDS) (D3514), and ruthenium red (RR) (84071) were obtained from Sigma-Aldrich. FLUO3-AM, 1,2-bis(*o*-aminophenoxy)ethane-*N*,*N*,*N*′,*N*′-tetraacetic acid tetra (acetoxymethyl) ester (BAPTA-AM) (196419), dantrolene (251680), and A23187 (A23) (100105) were purchased from Calbiochem. Acridine orange (AO), 3,3′-dihexyloxacarbocyanine iodide [$DiOC_6(3)$], and Rhod2-AM were purchased from Molecular Probes. Xestospongin C (XeC) (64950) was obtained from VWR Cayman. Mouse anti-cytochrome *c* antibody (556433) and mouse anti-actin antibody (A4700) were obtained from BD Pharmingen and Sigma-Aldrich, respectively. Horseradish peroxidase (HRP)-conjugated anti-mouse antibody (NA9310) was purchased from Amersham Biosciences.

Cell line, virus stock, and viral infection. Human neuroblastoma IMR5 cells (kindly provided by V. Yuste and S. Susin, Centre de Recherche des Cordeliers, Paris, France) and human HEp-2c cells (ATCC) were cultured in Dulbecco's modified Eagle's medium (DMEM) supplemented with 2 mM L-glutamine (Gibco) and 10% (vol/vol) heat-inactivated fetal bovine serum (FBS) (Gibco). Cells were maintained at 37°C in humidified air containing 95% air and 5% CO_2.

The attenuated vaccinal Sabin 2 strain of PV was used. Virus stocks were generated in HEp-2c cells and stored at −80°C until use. Virus titers were determined on HEp-2c and IMR5 cells by determining the number of 50% tissue culture infective doses ($TCID_{50}$) per ml, as described by Reed and Muench (28). Virus titers were similar in the two cell lines (data not shown). In all experiments, subconfluent IMR5 cell monolayers grown in 25-cm^2 flasks (TPP), in 24-well dishes (TPP), or in 6-well dishes (TPP) were inoculated with PV at a multiplicity of infection (MOI) of 50 $TCID_{50}$/cell in DMEM supplemented with 10% FBS, as previously described (3). Time zero postinfection (p.i.) corresponds to the time at which inoculation was performed.

In analyses of the apoptotic features of PV-infected cells, both adherent and detached cells were taken into account. Adherent cells were treated with EDTA or trypsin for Western blotting and flow cytofluorometry, respectively. They were

* Corresponding author. Mailing address: Institut Pasteur, Unité de Biologie des virus entériques, 25 rue du Dr Roux, 75015 Paris, France. Phone: 33 1 40 61 35 90. Fax: 33 1 40 61 33 67. E-mail: bruno.blondel@pasteur.fr.

† Present address: Trinity College, The Smurfit Institute, Molecular Cell Biology Laboratory, Dublin, Ireland.

▽ Published ahead of print on 22 September 2010.

collected with detached floating cells by centrifugation for 5 min at 500 × *g*. The cells were rinsed by centrifugation in phosphate-buffered saline (PBS) without calcium and analyzed as described below.

Flow cytofluorometry. Aliquots of 4×10^5 cells were used. Fluorescence was measured with a FACScan machine (Becton Dickinson). We analyzed at least 20,000 cells for each sample. Data were analyzed with Cellquest software (Becton Dickinson).

Cytosolic calcium measurement. The calcium-sensitive dye FLUO3-AM (excitation wavelength, 506 nm; emission wavelength, 526 nm) was used to measure the cytosolic calcium level. FLUO3-AM is almost nonfluorescent unless it is bound to calcium, and its fluorescence increases with rising calcium concentration (25). Cells were incubated in DMEM supplemented with 10% FBS and 1 μM FLUO3-AM, at 37°C, for 2 h before PV infection. At various times postinfection, cells were harvested, pelleted, and resuspended in ice-cold PBS containing 10 mM glucose and 10% FBS. Cytosolic calcium levels were determined by flow cytofluorometry.

Assessment of apoptosis. Cells were harvested, pelleted, and resuspended in ice-cold DMEM containing 10 μg/ml AO metachromatic nuclear dye (excitation wavelength, 500 nm; emission wavelength, 526 nm). The percentage of apoptotic cells was determined by flow cytofluorometry. Two populations of cells were separated, one consisting of living cells, characterized by bright AO fluorescence labeling, and the second corresponding to apoptotic cells, with a low fluorescence intensity (13).

Assessment of Δψm drop. Changes in the mitochondrial transmembrane potential (Δψm) were assessed by the flow cytofluorometry analysis of aliquots of 4×10^5 IMR5 cells stained with the potential-sensitive dye $DiOC_6(3)$ (excitation wavelength, 484 nm; emission wavelength, 501 nm) for 15 min at 4°C at a final concentration of 50 nM. $DiOC_6(3)$ fluorescence was measured by flow cytofluorometry. A drop in $DiOC_6(3)$ staining indicates the disruption of the mitochondrial membrane potential associated with apoptosis.

Mitochondrial calcium measurement and fluorescence staining. Rhod2-AM (excitation wavelength, 552 nm; emission wavelength, 581 nm) was used to measure the mitochondrial calcium level. The fluorescent dye Rhod2-AM has a net positive charge, facilitating its sequestration into mitochondria through membrane potential-driven uptake. The AM ester of the probe is cell permeant and rapidly cleaved in the mitochondria to yield the Rhod2 indicator, which displays a large increase in fluorescence intensity upon binding Ca^{2+} (32). For flow cytofluorometry, cells were harvested, pelleted, and resuspended in ice-cold PBS containing 10 mM glucose, 10% FBS, and 10 μM Rhod2-AM. Mitochondrial calcium levels were determined by the flow cytofluorometry analysis of aliquots of 4×10^5 cells. For fluorescence microscopy, IMR5 cells were grown on polylysine-coated (10 μg/ml) slides and stained with 7.5 μM Rhod2-AM in DMEM supplemented with 10% FBS for 2 h before PV infection. Cells were fixed by incubation for 15 min at 4°C in 4% paraformaldehyde. Cells were washed in PBS, and images were acquired with Zeiss Apotome and Axiovision software.

Subcellular fractionation. The subcellular proteome extraction kit (Calbiochem) was used to isolate the cytosolic fraction of IMR5 cells according to the manufacturer's instructions. Aliquots of 5×10^6 cells were harvested, pelleted, washed twice in PBS, resuspended in ice-cold extraction I buffer containing a protease inhibitor mixture, and incubated for 10 min at 4°C with gentle shaking. The suspension was centrifuged at 1,200 × *g* at 4°C for 10 min. The supernatant was used as the cytosolic fraction.

Western blot analysis. Protein concentrations were determined with the bicinchoninic acid protein assay kit (Pierce). Samples containing equal amounts of protein were subjected to sodium dodecyl sulfate-polyacrylamide gel electrophoresis (10 to 20% Tricine gels; Novex) as previously described (3). The proteins then were transferred to nitrocellulose membranes (Amersham Biosciences). Nonspecific sites were blocked as previously described (3), and the membranes were incubated for 2 h at room temperature with the primary antibody. Membranes then were washed in 0.1% Tween 20 in PBS (PBST; pH 7.4) and treated with the appropriate HRP-conjugated secondary antibody for 2 h at room temperature. The immunoblots were washed in PBST, and proteins were detected with an enhanced chemiluminescence detection kit (Amersham Biosciences) and a G-Box (SynGene). Anti-actin antibody was used to check for equal protein loading. The intensity of the bands was determined by densitometry.

Statistical analysis. Data are expressed as means ± standard errors of the means for three independent experiments. Student's *t* test was used to compare experimental conditions and controls. A *P* value of <0.05 was considered significant.

RESULTS AND DISCUSSION

PV induced an increase in cytosolic Ca^{2+} concentration that parallels PV-induced apoptosis. We first investigated whether PV modifies the cytosolic Ca^{2+} level in IMR5 cells. Cells were infected with PV at a multiplicity of infection (MOI) of 50 $TCID_{50}$ per cell. This MOI was used for all assays in this study. As a positive control for the analysis of cytosolic Ca^{2+} increases, cells were treated with TG (10 μM for 24 h), an inhibitor of ER Ca^{2+}-ATPase pumps leading to an accumulation of Ca^{2+} in the cytosol (31). Mock-infected cells were used as a negative control. The Ca^{2+}-sensitive dye FLUO3-AM was used to stain both adherent and detached cells for the determination of cytosolic Ca^{2+} levels by flow cytometry from 2 to 18 h p.i. Such pools of adherent and detached cells were used for all assays in this study. PV infection resulted in a time-dependent increase in the percentage of cells displaying an increase in cytosolic Ca^{2+}, reaching a plateau at 16 h p.i. (Fig. 1A and B).

We then compared the kinetics of the increase in cytosolic Ca^{2+} to those of PV-induced apoptosis, mitochondrial dysfunction ($\Delta\psi_m$ drop), and viral growth in PV-infected IMR5 cells. Apoptosis was analyzed at the indicated time points (Fig. 1C and D) until 18 h p.i. by measuring chromatin condensation and fragmentation by flow cytometry after being stained with the AO nuclear dye. $\Delta\psi_m$ drop was measured by flow cytometry in cells stained with the potential-sensitive dye $DiOC_6(3)$. The kinetics of the percentage of PV-infected cells displaying apoptosis or $\Delta\psi_m$ drop paralleled the kinetics of the percentage of cytosolic Ca^{2+} increase. The rate of virus synthesis reached a plateau at 8 h p.i. (Fig. 1E). For most of the other experiments presented, cells were monitored for 8 h, based on the cycle of virus synthesis.

An increase in cytosolic Ca^{2+} concentration is involved in PV-induced apoptosis. To investigate the possible role of cytosolic Ca^{2+} in the progression of PV-induced apoptosis, we used a permeant Ca^{2+} chelator, BAPTA-AM. Cells were left untreated or were treated with BAPTA-AM (15 μM) 2 h before PV infection. In all assays, including chelators or inhibitors, cells were treated 2 h before PV infection and drug concentrations were maintained throughout infection. Time zero p.i. corresponds to the time point at which inoculation was performed. Mock-infected cells, left untreated or treated with BAPTA-AM, were used as negative controls. We also checked that BAPTA-AM decreased cytosolic Ca^{2+} concentrations in PV-infected cells (Fig. 2A). Apoptosis was analyzed at 6 and 8 h p.i. after AO staining. BAPTA-AM significantly decreased the level of proapoptotic nuclear alterations induced by PV (Fig. 2B). We also analyzed the effect of BAPTA-AM on mitochondrial dysfunction, particularly as concerns $\Delta\psi_m$ drop and cytochrome *c* efflux from mitochondria to the cytosol, in a time course experiment. $\Delta\psi_m$ drop was measured by the flow cytometry analysis of cells stained with $DiOC_6(3)$. The drop in $\Delta\psi_m$ induced by PV was inhibited in cells treated with BAPTA-AM (Fig. 2C). Cytochrome *c* efflux into the cytosolic fraction was analyzed by Western blotting. Cytochrome *c* was detected in the cytoplasm of infected cells from 4 h p.i. (Fig. 2D). Cytochrome *c* release was clearly inhibited by BAPTA-AM in infected cells (Fig. 2D). Thus, an increase in cytosolic Ca^{2+} concentration appears to play a role in mi-

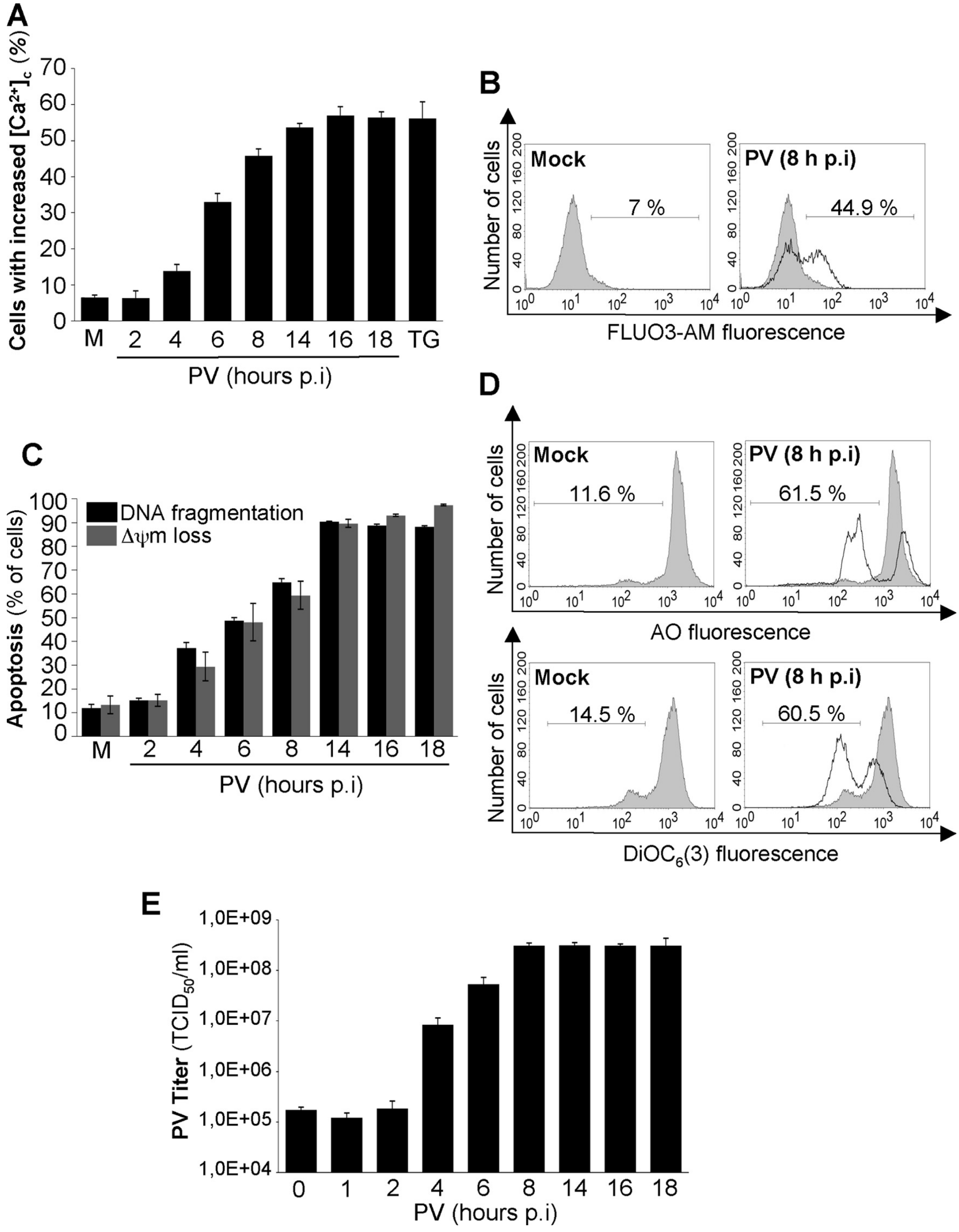

FIG. 1. PV-induced increase in cytosolic Ca^{2+} concentration and apoptosis and PV yield in IMR5 cells. (A) Time course of the increase in cytosolic Ca^{2+} concentration ($[Ca^{2+}]_c$) in PV-infected IMR5 cells. At the indicated times p.i., cytosolic Ca^{2+} levels were measured by flow cytometry with the Ca^{2+}-sensitive dye FLUO3-AM. Mock-infected (M) and TG-treated (TG) IMR5 cells were used as negative and positive controls, respectively. The graph shows the mean percentages of FLUO3-AM-fluorescent cells obtained from three independent experiments. Error bars indicate the standard errors of the means. (B) Representative flow cytometry histograms, after FLUO3-AM staining of mock-infected and PV-infected (8 h p.i.) IMR5 cells. The profiles of mock-infected control cells (gray area) and PV-infected cells (blank area) are shown. The percentages of FLUO3-AM-fluorescent cells are indicated for each of two experimental conditions. (C) Time course of apoptosis (DNA fragmentation and Δψm loss) in PV-infected IMR5 cells. Mock-infected (M) and PV-infected IMR5 cells were analyzed at the indicated times p.i. by flow cytometry after being stained with the nuclear dye AO or $DiOC_6(3)$ to assess DNA fragmentation and Δψm loss, respectively. The graph shows the means, from three independent experiments, of the percentages of cells with fragmented DNA (black) and cells with Δψm loss (gray). Error bars indicate the standard errors of the means. (D) Representative flow cytometry histograms after AO (top) or $DiOC_6(3)$ (bottom) staining of mock-infected and PV-infected (8 h p.i.) IMR5 cells. The profiles of mock-infected control cells (gray area) and PV-infected cells (blank area) are shown. The percentages of apoptotic cells, with a low fluorescence intensity, are indicated for each set of experimental conditions. (E) One-step growth curve of PV in IMR5 cells. Cells and supernatants were harvested at the indicated times p.i. and subjected to three cycles of freezing and thawing. Total virus yields were determined by $TCID_{50}$ assays. Each point represents the mean virus titer for three independent experiments. Error bars indicate the standard errors of the means.

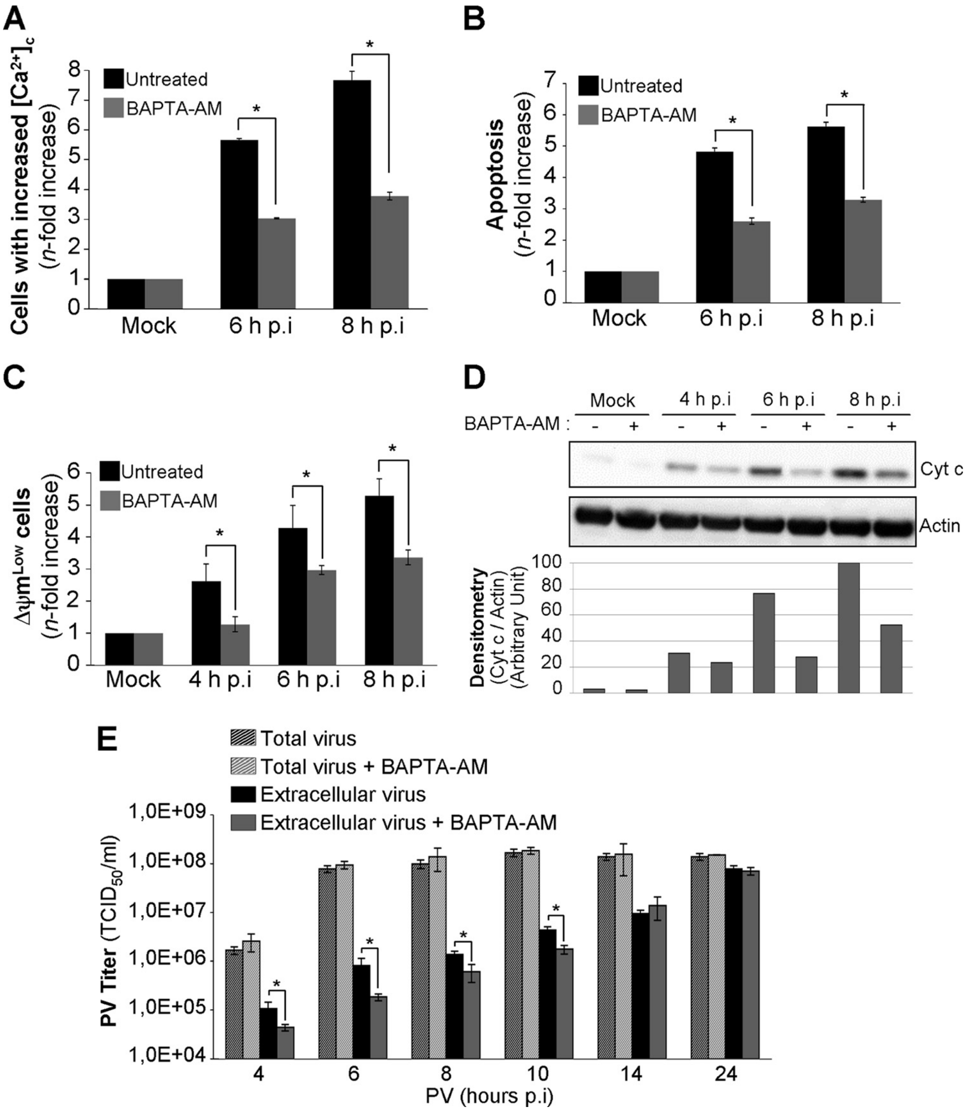

FIG. 2. Treatment of cells with the intracellular Ca^{2+} chelator BAPTA-AM decreases PV-induced apoptosis and PV externalization in IMR5 cells. (A) Smaller increase in cytosolic Ca^{2+} concentration ($[Ca^{2+}]_c$) in PV-infected IMR5 cells treated with the intracellular Ca^{2+} chelator BAPTA-AM. Mock-infected and PV-infected IMR5 cells treated with 15 μM BAPTA-AM (gray) or not treated (black) were analyzed at the indicated times p.i. by flow cytometry after FLUO3-AM staining. The increase (*n*-fold) in cytosolic Ca^{2+} was calculated as the ratio of the percentage of fluorescent PV-infected IMR5 cells to the percentage of fluorescent mock-infected cells. The data shown are the means from three independent experiments. Error bars indicate the standard errors of the means. *, $P < 0.05$ by Student's *t* test comparing untreated IMR5 cells to treated IMR5 cells. (B) Decrease in apoptosis in PV-infected cells treated with BAPTA-AM. Mock-infected and PV-infected IMR5 cells, treated with BAPTA-AM (15 μM) (gray) or not treated (black), were analyzed at the indicated times p.i. by flow cytometry after AO staining. The increase (*n*-fold) in apoptosis was calculated as the ratio of the percentage of apoptotic PV-infected IMR5 cells to the percentage of apoptotic mock-infected cells. The data shown are the means from three independent experiments. Error bars indicate the standard errors of the means. *, $P < 0.05$ by Student's *t* test comparing untreated IMR5 cells to treated IMR5 cells. (C) Decrease in Δψm drop in PV-infected cells treated with BAPTA-AM. Mock-infected and PV-infected IMR5 cells treated with 15 μM BAPTA-AM (gray) or not treated (black) were analyzed at the indicated times p.i. by flow cytometry after $DiOC_6(3)$ staining. The increase (*n*-fold) in apoptosis was calculated as the ratio of the percentage of apoptotic PV-infected IMR5 cells ($\Delta\psi m^{Low}$) to the percentage of apoptotic mock-infected cells. The data shown are the means from three independent experiments. Error bars indicate the standard errors of the means. *, $P < 0.05$ by Student's *t* test comparing untreated IMR5 cells to treated IMR5 cells. (D) Decrease in cytochrome *c* release in PV-infected cells treated with BAPTA-AM. Cells were mock infected or infected with PV in the presence or absence of BAPTA-AM (15 μM). At the indicated times p.i., cells were collected and subjected to subcellular fractionation. Cytochrome *c* (Cyt c) was detected in the cytosolic fraction by Western blotting with an anti-cytochrome *c* antibody. Actin was used as a protein-loading control. Protein levels were determined by densitometry and plotted as ratios relative to actin levels. (E) Effect of BAPTA-AM on viral growth and PV externalization. IMR5 cells were infected with PV in the presence or absence of BAPTA-AM (15 μM). The total virus yield (extracellular and intracellular) was determined by $TCID_{50}$ assay at the indicated times after three cycles of freezing and thawing to release intracellular viruses. The extracellular virus titers were determined from the supernatant of PV-infected cells at the indicated times after the removal of detached cells by centrifugation. Each point represents the mean virus titer for three independent experiments. Error bars indicate the standard errors of the means. *, $P < 0.05$ by Student's *t* test comparing untreated IMR5 cells to treated IMR5 cells.

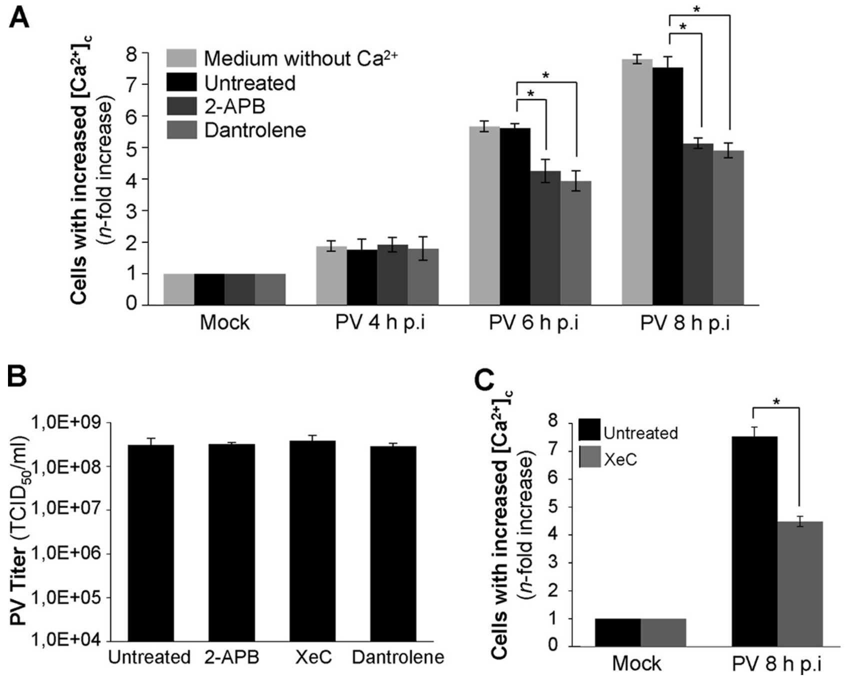

FIG. 3. PV induces Ca^{2+} release from the ER through IP_3R and RyR channels in IMR5 cells. (A) Smaller increase in the cytosolic Ca^{2+} concentration ($[Ca^{2+}]_c$) in PV-infected IMR5 cells treated with the IP_3R channel inhibitor 2-APB or the RyR inhibitor dantrolene. Cells were mock infected or infected with PV in medium without Ca^{2+} (light gray) or in medium with Ca^{2+} in the presence of 10 μM 2-APB (dark gray) or 20 μM dantrolene (gray) or in the absence of inhibitor (black). At the indicated times p.i., cells were analyzed by flow cytometry after FLUO3-AM staining. The increase (*n*-fold) in cytosolic Ca^{2+} was calculated as the ratio of the percentage of fluorescent PV-infected IMR5 cells to the percentage of fluorescent mock-infected cells. The data shown are the means from three independent experiments. Error bars indicate the standard errors of the means. *, $P < 0.05$ by Student's *t* test comparing untreated IMR5 cells to treated IMR5 cells. (B) The treatment of IMR5 cells with 2-APB, XeC, or dantrolene does not affect PV growth. IMR5 cells were infected with PV for 8 h in the presence or absence of 2-APB (10 μM), XeC (10 μM), or dantrolene (20 μM). Total virus yield (extracellular and intracellular) was determined by $TCID_{50}$ assay after three cycles of freezing and thawing to release intracellular viruses. Each point represents the mean virus titers for three independent experiments. Error bars indicate the standard errors of the means. (C) Smaller increase in cytosolic Ca^{2+} concentration ($[Ca^{2+}]_c$) in PV-infected IMR5 cells treated with the IP_3R channel inhibitor XeC. Mock-infected and PV-infected (8 h p.i.) IMR5 cells treated with 10 μM XeC (gray) or left untreated (black) were analyzed at the indicated times p.i. by flow cytometry after FLUO3-AM staining. The increase (*n*-fold) in cytosolic Ca^{2+} was calculated as the ratio of the percentage of fluorescent PV-infected IMR5 cells to the percentage of fluorescent mock-infected cells. The data shown are the means from three independent experiments. Error bars indicate the standard errors of the means. *, $P < 0.05$ by Student's *t* test comparing untreated IMR5 cells to treated IMR5 cells.

tochondrial dysfunction and apoptosis following the PV infection of IMR5 cells.

We then evaluated the effect of an increase in cytosolic Ca^{2+} on the amount of virus produced in IMR5 cells by determining the kinetics of total virus yield in the presence or absence of BAPTA-AM. The Ca^{2+} chelator had no effect on the total amount of virus produced (Fig. 2E). We previously showed that PV-induced apoptosis is involved in virus release (2, 3). As PV-induced apoptosis levels were lower in infected cells treated with BAPTA-AM than in untreated cells (Fig. 2B), we assessed the possible effects of this decrease on virus release. Virus release was delayed until 10 h p.i. in the presence of BAPTA-AM (Fig. 2E). From 14 h p.i. onwards, virus release was similar in the presence and absence of BAPTA-AM, probably because of high apoptosis levels.

Thus, an increase in cytosolic Ca^{2+} concentration appears to play a role in viral release without affecting virus production, as previously observed in cells infected with another enterovirus, coxsackievirus B (CVB) (34).

Ca^{2+} is released from the ER in PV-infected cells. The increase in cytosolic Ca^{2+} may be due to an influx of Ca^{2+} from the extracellular medium across the plasma membrane and/or Ca^{2+} release from intracellular stores, predominantly from the ER. Irurzun et al. (20) previously showed that at least some of the cytosolic Ca^{2+} in PV-infected cells is transported from the external medium, through voltage-sensitive Ca^{2+} channels. However, the increase in cytosolic Ca^{2+} in Ca^{2+}-free medium indicates that intracellular stores also provide cytosolic Ca^{2+} (20).

We investigated the role of extracellular Ca^{2+} in the increase in cytosolic Ca^{2+} concentration during PV infection in IMR5 cells by analyzing cytosolic Ca^{2+} levels in cells placed in a medium without Ca^{2+} for 2 h before and throughout PV infection. The increase in cytosolic Ca^{2+} was similar in media with and without Ca^{2+} at 4, 6, and 8 h p.i. (Fig. 3A). Thus, extracellular calcium does not seem to be involved in the increase in cytosolic Ca^{2+} in our model.

Van Kuppeveld's group previously demonstrated that a channel formed by the PV nonstructural protein 2B may be involved in Ca^{2+} release from ER stores into the cytosol (10). We investigated whether the increase in cytosolic Ca^{2+} concentration during PV infection in IMR5 cells also was due to

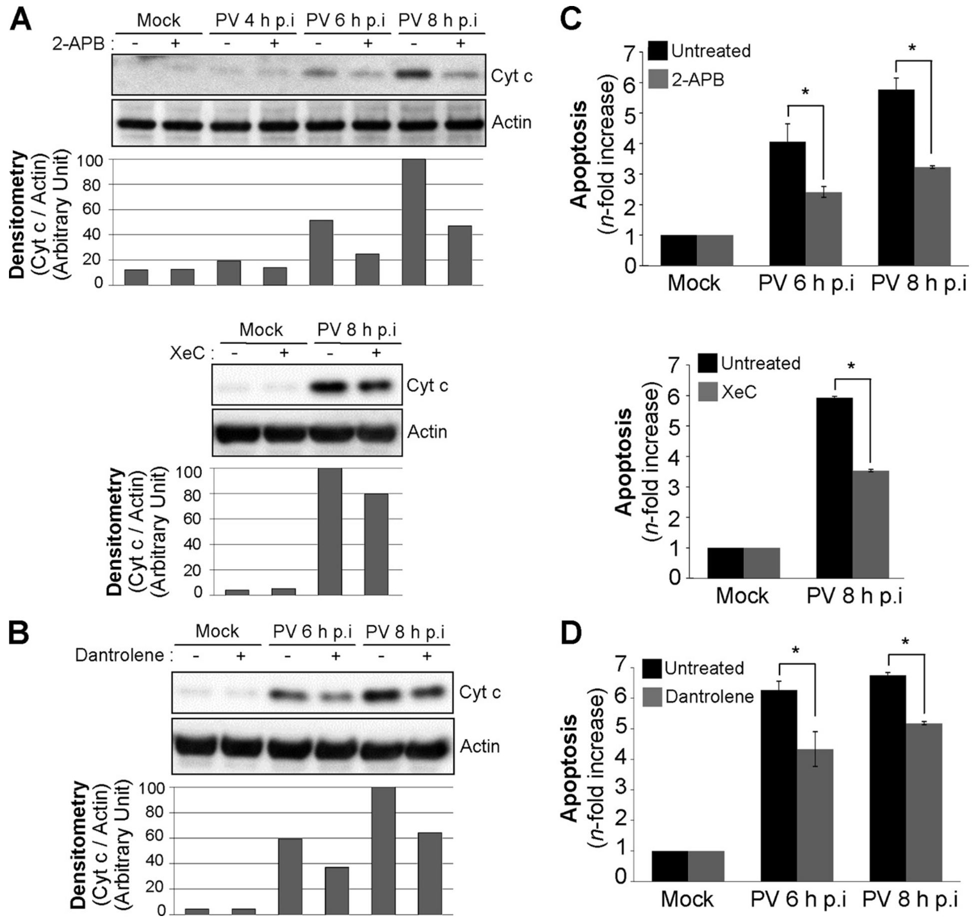

FIG. 4. Inhibition of IP_3R and RyR channels decreases PV-induced cytochrome *c* release and apoptosis in IMR5 cells. (A) Decrease in cytochrome *c* release in PV-infected IMR5 cells treated with the IP_3R channel inhibitor 2-APB or XeC. Cells were mock infected or infected with PV in the presence or absence of 10 μM 2-APB (top) or 10 μM XeC (bottom). At the indicated times p.i., cells were collected and subjected to subcellular fractionation. Cytochrome *c* (Cyt c) was detected in the cytosolic fraction by Western blotting with an anti-cytochrome *c* antibody. Actin was used as a protein-loading control. Protein levels were determined by densitometry and plotted as ratios relative to the actin levels. (B) Decrease in cytochrome *c* release in PV-infected IMR5 cells treated with the RyR channel inhibitor dantrolene. Cells were mock infected or infected with PV in the presence or absence of 20 μM dantrolene. At the indicated times p.i., cells were collected and subjected to subcellular fractionation. Cytochrome *c* was detected in the cytosolic fraction by Western blotting with an anti-cytochrome *c* antibody. Actin was used as a protein-loading control. Protein levels were determined by densitometry and plotted as ratios relative to the actin levels. (C) Decrease in apoptosis in PV-infected cells treated with 2-APB or XeC. Mock-infected and PV-infected IMR5 cells were left untreated (black) or were treated (gray) with 10 μM 2-APB (top) or 10 μM XeC (bottom). At the indicated times p.i., cells were analyzed by flow cytometry after AO staining. The increase (*n*-fold) in apoptosis was calculated as the ratio of the percentage of apoptotic PV-infected IMR5 cells to the percentage of apoptotic mock-infected cells. The data shown are the means from three independent experiments. Error bars indicate the standard errors of the means. ∗, $P < 0.05$ by Student's *t* test comparing untreated IMR5 cells to treated IMR5 cells. (D) Decrease in apoptosis in PV-infected cells treated with dantrolene. Mock-infected and PV-infected IMR5 cells were left untreated (black) or were treated with 20 μM dantrolene (gray). At the indicated times p.i., cells were analyzed by flow cytometry after AO staining. The increase (*n*-fold) in apoptosis was calculated as the ratio of the percentage of apoptotic PV-infected IMR5 cells to the percentage of apoptotic mock-infected cells. The data shown are the means from three independent experiments. Error bars indicate the standard errors of the means. ∗, $P < 0.05$ by Student's *t* test comparing untreated IMR5 cells to treated IMR5 cells.

the release of Ca^{2+} from the ER through the IP_3R and/or RyR channels, which have been implicated in apoptotic Ca^{2+} signaling between intracellular stores and mitochondria in several models (7, 12, 15). We therefore treated cells with inhibitors of these receptors, 2-APB (10 μM) and dantrolene (20 μM), respectively. We checked that 2-APB and dantrolene had no effect on PV yield at the concentrations used (Fig. 3B). Mock-infected cells, left untreated or treated with 2-APB or dantrolene, were used as negative controls. Cytosolic Ca^{2+} levels were analyzed at 4, 6, and 8 h p.i. (Fig. 3A). The inhibition of Ca^{2+} release from the ER by 2-APB or dantrolene resulted in lower cytosolic Ca^{2+} concentration. Thus, Ca^{2+} release from the ER lumen through the IP_3R and RyR channels seems to be involved in the increase in cytosolic Ca^{2+} concentration during PV infection. For the confirmation of the role of IP_3R in the release of Ca^{2+} from the ER following PV infection, we used another IP_3R inhibitor, XeC (10 μM) (14). We first checked that XeC had no effect on PV yield at the concentration used (Fig. 3B). This inhibitor decreased cytosolic Ca^{2+} concentration to an extent similar to that of 2-APB (Fig. 3C). This result provides further evidence that IP_3R is involved in the release of Ca^{2+} from the ER following PV infection.

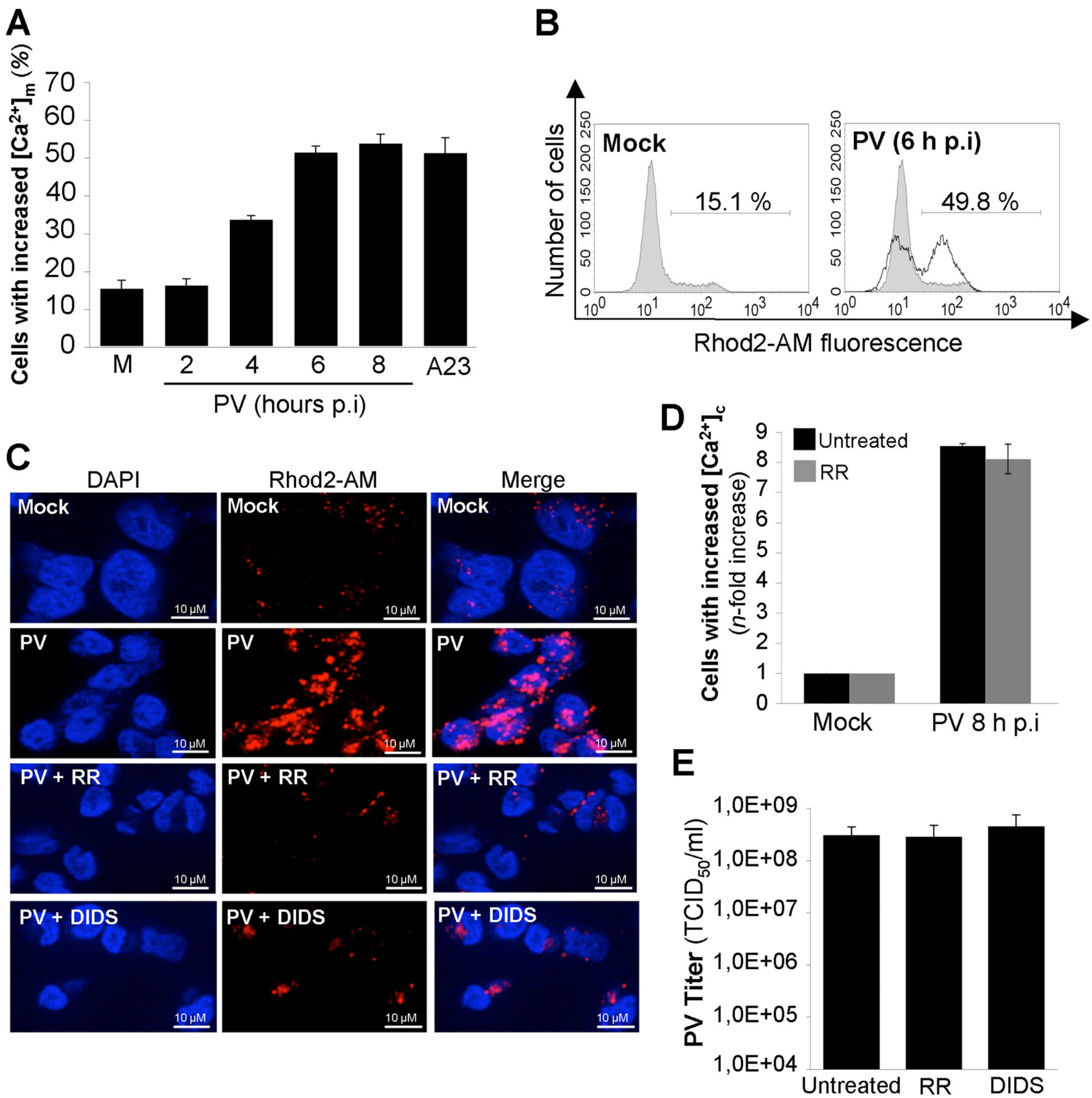

FIG. 5. PV induces mitochondrial Ca^{2+} uptake via the mitochondrial Ca^{2+} uniporter and VDAC in IMR5 cells. (A) Time course of the increase in mitochondrial Ca^{2+} concentration ($[Ca^{2+}]_m$) in PV-infected IMR5 cells. At the indicated times p.i., mitochondrial Ca^{2+} levels were measured by flow cytometry with Rhod2-AM. Mock-infected (M) and A23-treated (A23) IMR5 cells were used as negative and positive controls, respectively. The graph shows the mean percentages of Rhod2-AM-fluorescent cells obtained from three independent experiments. Error bars indicate the standard errors of the means. (B) Representative flow cytometry histograms after Rhod2-AM staining of mock-infected and PV-infected (6 h p.i.) IMR5 cells. The profiles of mock-infected control cells (gray area) and PV-infected cells (blank area) are shown. The percentages of Rhod2-AM-fluorescent cells for each of two experimental conditions are indicated. (C) Reduction of mitochondrial Ca^{2+} level in PV-infected IMR5 cells treated with RR or DIDS, antagonists of the mitochondrial Ca^{2+} uniporter and VDAC, respectively. IMR5 cells were mock infected or infected with PV (6 h p.i.) in the presence or absence of RR (2 μM) or DIDS (10 μM). Cells were analyzed by fluorescence microscopy after Rhod2-AM staining (red; middle). Nuclei were stained with 4′,6-diamidino-2-phenylindole (DAPI; blue; left). The merged image is an overlay of the DAPI and Rhod2-AM images (right). (D) The treatment of IMR5 cells with RR does not affect the PV-induced increase in cytosolic Ca^{2+} concentration ($[Ca^{2+}]_c$). Mock-infected and PV-infected (8 h p.i.) IMR5 cells treated with 2 μM RR (gray) or not treated (black) were analyzed by flow cytometry after FLUO3-AM staining. The increase (*n*-fold) in cytosolic Ca^{2+} was calculated as the ratio of the percentage of fluorescent PV-infected IMR5 cells to the percentage of fluorescent mock-infected cells. The data shown are the means from three independent experiments. Error bars indicate the standard errors of the means. *, $P < 0.05$ by Student's *t* test comparing untreated IMR5 cells to treated IMR5 cells. (E) The treatment of IMR5 cells with RR or DIDS does not affect PV growth in IMR5 cells. IMR5 cells were infected with PV for 8 h in the presence or absence of RR (2 μM) or DIDS (10 μM). Total virus yield (extracellular and intracellular) was determined by $TCID_{50}$ assay after three cycles of freezing and thawing to release intracellular viruses. Each point represents the mean virus titers for three independent experiments. Error bars indicate the standard errors of the means.

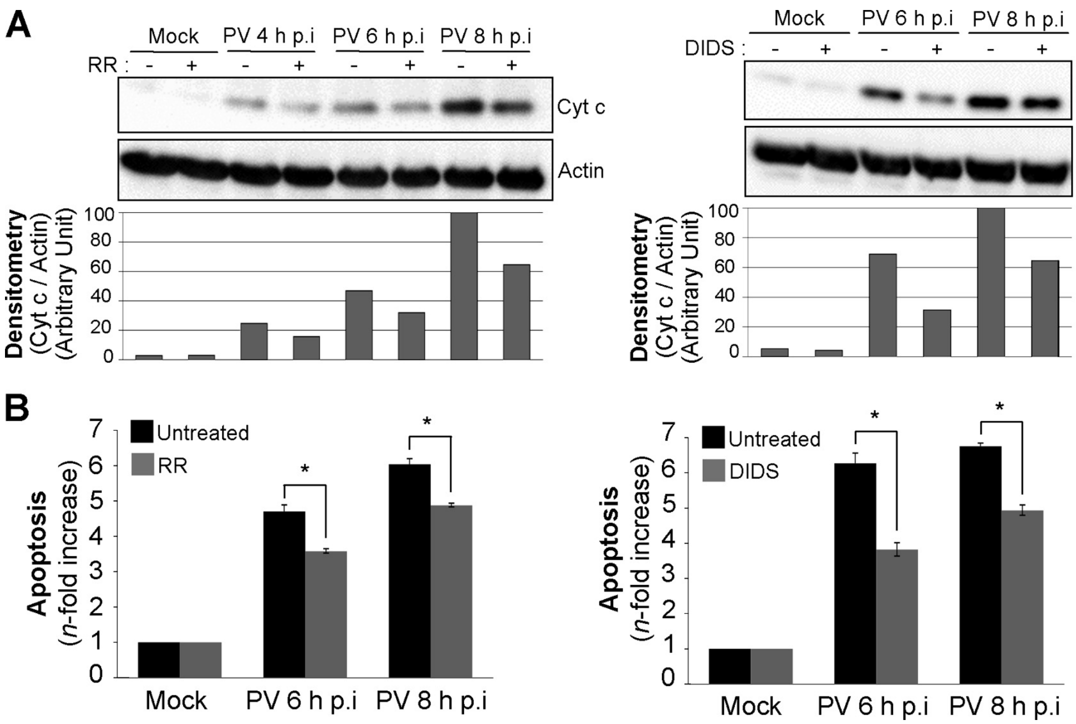

FIG. 6. Inhibition of mitochondrial Ca^{2+} uptake following PV infection decreases cytochrome *c* release and apoptosis in IMR5 cells. (A) Decrease in cytochrome *c* release in PV-infected cells treated with RR or DIDS. Cells were mock infected or infected with PV in the presence or absence of 2 μM RR (left) or 10 μM DIDS (right). At the indicated times p.i., cells were collected and subjected to subcellular fractionation. Cytochrome *c* (Cyt c) was detected in the cytosolic fraction by Western blotting with an anti-cytochrome *c* antibody. Actin was used as a protein-loading control. Protein levels were determined by densitometry and plotted as ratios relative to actin levels. (B) Decrease in apoptosis in PV-infected IMR5 cells treated with RR or DIDS. Mock- and PV-infected IMR5 cells were left untreated (black) or were treated (gray) with 2 μM RR (left) or 10 μM DIDS (right). At the indicated times p.i., cells were analyzed by flow cytometry after AO staining, and the increase (*n*-fold) in apoptosis was calculated as the ratio of the percentage of apoptotic PV-infected IMR5 cells to the percentage of apoptotic mock-infected cells. The data shown are the means from three independent experiments. Error bars indicate the standard errors of the means. *, $P < 0.05$ by Student's *t* test comparing untreated IMR5 cells to treated IMR5 cells.

Ca^{2+} release from the ER is involved in PV-induced apoptosis. We investigated the possible role of Ca^{2+} release from the ER in mitochondrial dysfunction in infected IMR5 cells by analyzing cytochrome *c* efflux from mitochondria at 4, 6, and 8 h p.i. in the cytosolic fraction of cells left untreated or treated with 2-APB, XeC, or dantrolene. Cytochrome *c* release was clearly inhibited in cells infected with PV in the presence of 2-APB, XeC, or dantrolene (Fig. 4A and B). Similarly, all three inhibitors clearly decreased the level of DNA fragmentation (Fig. 4C and D).

Thus, Ca^{2+} release from the ER through the IP_3R and RyR channels is involved in PV-induced mitochondrial dysfunction and apoptosis.

Ca^{2+} translocation into mitochondria plays a role in PV-induced apoptosis. We then investigated the mechanism by which Ca^{2+} released from the ER contributed to apoptosis in PV-infected IMR5 cells. As mentioned above, Ca^{2+} exchange between the ER and mitochondria can play a key role in apoptosis (7, 12, 15). Ca^{2+} influx into mitochondria was assessed in PV-infected cells, with the fluorescent, mitochondrial probe Rhod2-AM (32). Mitochondrial Ca^{2+} uptake was determined in mock- and PV-infected cells from 2 to 8 h p.i. by flow cytometry. The Ca^{2+} ionophore A23 (10 μM for 1 h) was used as a positive control to induce the influx of Ca^{2+} into mitochondria in uninfected cells (12). PV infection resulted in a time-dependent increase in the percentage of cells displaying an increase in mitochondrial Ca^{2+} (Fig. 5A and B). A high concentration of Ca^{2+} in mitochondria also was illustrated by punctate labeling in cells, which is consistent with the location of Ca^{2+} in the mitochondria following fluorescence staining with Rhod2-AM at 6 h p.i. (Fig. 5C).

Two major mitochondrial actors mediating Ca^{2+} signaling delivery between the ER and mitochondria are the Ca^{2+} uniporter (29) and the voltage-dependent anion channel (VDAC) (9). We investigated the involvement of these channels in mitochondrial Ca^{2+} uptake during PV-induced apoptosis by treating cells with RR (2 μM), a noncompetitive inhibitor of the mitochondrial Ca^{2+} uniporter (35), or with the VDAC inhibitor DIDS (10 μM), which inhibits Ca^{2+} influx into mitochondria (24). We checked that RR did not inhibit the increase in cytosolic Ca^{2+} in PV-infected cells (Fig. 5D). This molecule therefore did not inhibit IP_3R or RyR in our model, in contrast to results of certain other reports (21). We also checked that RR and DIDS had no effect on PV yield at the concentrations used (Fig. 5E). The inhibition of mitochondrial Ca^{2+} uptake by RR or DIDS in IMR5 cells infected with PV was illustrated following fluorescence staining with Rhod2-AM at 6 h p.i. (Fig. 5C).

Cytochrome *c* release from mitochondria in PV-infected cells with or without RR or DIDS treatment was analyzed by

Western blotting on the cytosolic fraction at 4, 6, and 8 h p.i. Mock-infected cells, left untreated or treated with RR or DIDS, were used as negative controls. Cytochrome *c* efflux was partially inhibited in infected cells by RR or DIDS (Fig. 6A). The level of PV-induced apoptosis accordingly decreased in cells treated with RR or DIDS (Fig. 6B).

Thus, mitochondrial Ca^{2+} uptake through the Ca^{2+} uniporter and VDAC plays a role in PV-induced apoptosis in IMR5 cells.

Mitochondria take up Ca^{2+} released from the ER through the IP_3R and RyR channels, but other routes may be involved in Ca^{2+} release from the ER in cells infected with enteroviruses (20, 34). Van Kuppeveld's group has shown that the individual expression of the nonstructural protein 2B from CVB or PV in HeLa cells induces Ca^{2+} release from both ER and Golgi stores (6, 10, 11). 2B is a viroporin that forms pores in membranes (1, 33). Interestingly, CVB 2B has an antiapoptotic effect (6, 33). The 2B protein may downregulate apoptotic Ca^{2+} signaling between the ER and mitochondria by decreasing the amount of Ca^{2+} stored in the ER, thereby decreasing Ca^{2+} release through IP_3R and RyR and its uptake by mitochondria. Indeed, the Ca^{2+} released via 2B channels is not taken up by the mitochondria, which take up Ca^{2+} principally at ER-mitochondrial junctions. The 2B protein therefore may delay the PV-induced apoptotic program, providing the virus with sufficient time to replicate. Using a different cell system, Madan et al. (23) showed that PV 2B also was associated with mitochondria and had a proapoptotic effect, inducing mitochondrial dysfunction in BHK-21 cells.

The role of Ca^{2+} in the regulation of PV-induced apoptosis therefore is complex. Ca^{2+} may modulate several signaling pathways involved in the pro-/antiapoptotic balance described by Agol's group in enterovirus-infected cells (4).

Our study provides new insight into these processes by showing that PV infection induces an increase in cytosolic Ca^{2+} concentration, at least partly through Ca^{2+} release from the ER lumen via the IP_3R and RyR channels, leading to Ca^{2+} accumulation in the mitochondria via the mitochondrial Ca^{2+} uniporter and VDAC. It also shows that this increase in mitochondrial Ca^{2+} concentration in PV-infected cells contributes to mitochondrial dysfunction and apoptosis.

ACKNOWLEDGMENTS

We thank Barbara Maison for valuable advice on fluorescence assays and V. Youste and S. Susin (Centre de Recherche des Cordeliers, Paris, France) for providing IMR5 cells.

This study was supported by grants from the Institut Pasteur (Transverse research program PTR 276), the Agence Nationale de la Recherche (ANR-09-MIEN-019), and the Fondation pour la Recherche Médicale (DMI20091117313). C.B. was supported by grants from the Ministère de l'Enseignement Supérieur et de la Recherche.

REFERENCES

1. **Agirre, A., A. Barco, L. Carrasco, and J. L. Nieva.** 2002. Viroporin-mediated membrane permeabilization. Pore formation by nonstructural poliovirus 2B protein. J. Biol. Chem. **277:**40434–40441.
2. **Autret, A., S. Martin-Latil, C. Brisac, L. Mousson, F. Colbère-Garapin, and B. Blondel.** 2008. Early phosphatidylinositol 3-kinase/Akt pathway activation limits poliovirus-induced JNK-mediated cell death. J. Virol. **82:**3796–3802.
3. **Autret, A., S. Martin-Latil, L. Mousson, A. Wirotius, F. Petit, D. Arnoult, F. Colbère-Garapin, J. Estaquier, and B. Blondel.** 2007. Poliovirus induces Bax-dependent cell death mediated by c-Jun NH2-terminal kinase. J. Virol. **81:**7504–7516.
4. **Belov, G. A., L. I. Romanova, E. A. Tolskaya, M. S. Kolesnikova, Y. A. Lazebnik, and V. I. Agol.** 2003. The major apoptotic pathway activated and suppressed by poliovirus. J. Virol. **77:**45–56.
5. **Blondel, B., A. Autret, C. Brisac, S. Martin-Latil, L. Mousson, I. Pelletier, J. Estaquier, and F. Colbère-Garapin.** 2009. Apoptotic signaling cascades operating in poliovirus-infected cells. Front. Biosci. **14:**2181–2192.
6. **Campanella, M., A. S. de Jong, K. W. Lanke, W. J. Melchers, P. H. Willems, P. Pinton, R. Rizzuto, and F. J. van Kuppeveld.** 2004. The coxsackievirus 2B protein suppresses apoptotic host cell responses by manipulating intracellular Ca2+ homeostasis. J. Biol. Chem. **279:**18440–18450.
7. **Celsi, F., P. Pizzo, M. Brini, S. Leo, C. Fotino, P. Pinton, and R. Rizzuto.** 2009. Mitochondria, calcium and cell death: a deadly triad in neurodegeneration. Biochim. Biophys. Acta **1787:**335–344.
8. **Chami, M., B. Oules, and P. Paterlini-Brechot.** 2006. Cytobiological consequences of calcium-signaling alterations induced by human viral proteins. Biochim. Biophys. Acta **1763:**1344–1362.
9. **Colombini, M.** 1979. A candidate for the permeability pathway of the outer mitochondrial membrane. Nature **279:**643–645.
10. **de Jong, A. S., F. de Mattia, M. M. Van Dommelen, K. Lanke, W. J. Melchers, P. H. Willems, and F. J. van Kuppeveld.** 2008. Functional analysis of picornavirus 2B proteins: effects on calcium homeostasis and intracellular protein trafficking. J. Virol. **82:**3782–3790.
11. **de Jong, A. S., H. J. Visch, F. de Mattia, M. M. van Dommelen, H. G. Swarts, T. Luyten, G. Callewaert, W. J. Melchers, P. H. Willems, and F. J. van Kuppeveld.** 2006. The coxsackievirus 2B protein increases efflux of ions from the endoplasmic reticulum and Golgi, thereby inhibiting protein trafficking through the Golgi. J. Biol. Chem. **281:**14144–14150.
12. **Deniaud, A., O. Sharaf el Dein, E. Maillier, D. Poncet, G. Kroemer, C. Lemaire, and C. Brenner.** 2008. Endoplasmic reticulum stress induces calcium-dependent permeability transition, mitochondrial outer membrane permeabilization and apoptosis. Oncogene **27:**285–299.
13. **Estaquier, J., T. Idziorek, F. de Bels, F. Barre-Sinoussi, B. Hurtrel, A. M. Aubertin, A. Venet, M. Mehtali, E. Muchmore, P. Michel, Y. Mouton, M. Girard, and J. C. Ameisen.** 1994. Programmed cell death and AIDS: significance of T-cell apoptosis in pathogenic and nonpathogenic primate lentiviral infections. Proc. Natl. Acad. Sci. U. S. A. **91:**9431–9435.
14. **Gafni, J., J. A. Munsch, T. H. Lam, M. C. Catlin, L. G. Costa, T. F. Molinski, and I. N. Pessah.** 1997. Xestospongins: potent membrane permeable blockers of the inositol 1,4,5-trisphosphate receptor. Neuron **19:**723–733.
15. **Giorgi, C., D. De Stefani, A. Bononi, R. Rizzuto, and P. Pinton.** 2009. Structural and functional link between the mitochondrial network and the endoplasmic reticulum. Int. J. Biochem. Cell Biol. **41:**1817–1827.
16. **Girard, S., T. Couderc, J. Destombes, D. Thiesson, F. Delpeyroux, and B. Blondel.** 1999. Poliovirus induces apoptosis in the mouse central nervous system. J. Virol. **73:**6066–6072.
17. **Gosselin, A. S., Y. Simonin, F. Guivel-Benhassine, V. Rincheval, J. L. Vayssiere, B. Mignotte, F. Colbère-Garapin, T. Couderc, and B. Blondel.** 2003. Poliovirus-induced apoptosis is reduced in cells expressing a mutant CD155 selected during persistent poliovirus infection in neuroblastoma cells. J. Virol. **77:**790–798.
18. **Griffin, D. E. (ed.).** 2005. Role of apoptosis in infection, vol. 289. Springer, Heidelberg, Germany.
19. **Guinea, R., A. Lopez-Rivas, and L. Carrasco.** 1989. Modification of phospholipase C and phospholipase A2 activities during poliovirus infection. J. Biol. Chem. **264:**21923–21927.
20. **Irurzun, A., J. Arroyo, A. Alvarez, and L. Carrasco.** 1995. Enhanced intracellular calcium concentration during poliovirus infection. J. Virol. **69:**5142–5146.
21. **Koulen, P., and E. C. Thrower.** 2001. Pharmacological modulation of intracellular Ca(2+) channels at the single-channel level. Mol. Neurobiol. **24:**65–86.
22. **Kroemer, G., L. Galluzzi, and C. Brenner.** 2007. Mitochondrial membrane permeabilization in cell death. Physiol. Rev. **87:**99–163.
23. **Madan, V., A. Castello, and L. Carrasco.** 2008. Viroporins from RNA viruses induce caspase-dependent apoptosis. Cell Microbiol. **10:**437–451.
24. **Madesh, M., and G. Hajnoczky.** 2001. VDAC-dependent permeabilization of the outer mitochondrial membrane by superoxide induces rapid and massive cytochrome *c* release. J. Cell Biol. **155:**1003–1015.
25. **Minta, A., J. P. Kao, and R. Y. Tsien.** 1989. Fluorescent indicators for cytosolic calcium based on rhodamine and fluorescein chromophores. J. Biol. Chem. **264:**8171–8178.
26. **Pallansch, M., and R. Roos.** 2007. Enteroviruses: polioviruses, coxsackieviruses, echoviruses, and newer enteroviruses, p. 839–893. *In* D. M. Knipe and P. M. Howley (ed.), Fields virology, vol. 1. Lippincott Williams and Wilkins, Philadelphia, PA.
27. **Racaniello, V. R.** 2007. Picornaviridae: the viruses and their replication, p. 795–838. *In* D. M. Knipe and P. M. Howley (ed.), Fields virology, 4th ed., vol. 1. Lippincott Williams and Wilkins, Philadelphia, PA.
28. **Reed, L. J., and M. Muench.** 1938. A simple method for estimating fifty percent endpoints. Am. J. Hyg. (London) **27:**493–497.
29. **Rizzuto, R., P. Pinton, W. Carrington, F. S. Fay, K. E. Fogarty, L. M. Lifshitz, R. A. Tuft, and T. Pozzan.** 1998. Close contacts with the endoplasmic reticulum as determinants of mitochondrial Ca2+ responses. Science **280:**1763–1766.

30. **Szegezdi, E., S. E. Logue, A. M. Gorman, and A. Samali.** 2006. Mediators of endoplasmic reticulum stress-induced apoptosis. EMBO Rep. **7:**880–885.
31. **Thastrup, O., P. J. Cullen, B. K. Drobak, M. R. Hanley, and A. P. Dawson.** 1990. Thapsigargin, a tumor promoter, discharges intracellular Ca2+ stores by specific inhibition of the endoplasmic reticulum Ca2(+)-ATPase. Proc. Natl. Acad. Sci. U. S. A. **87:**2466–2470.
32. **Trollinger, D. R., W. E. Cascio, and J. J. Lemasters.** 1997. Selective loading of Rhod 2 into mitochondria shows mitochondrial Ca2+ transients during the contractile cycle in adult rabbit cardiac myocytes. Biochem. Biophys. Res. Commun. **236:**738–742.
33. **van Kuppeveld, F. J., A. S. de Jong, W. J. Melchers, and P. H. Willems.** 2005. Enterovirus protein 2B po(u)res out the calcium: a viral strategy to survive? Trends Microbiol. **13:**41–44.
34. **van Kuppeveld, F. J., J. G. Hoenderop, R. L. Smeets, P. H. Willems, H. B. Dijkman, J. M. Galama, and W. J. Melchers.** 1997. Coxsackievirus protein 2B modifies endoplasmic reticulum membrane and plasma membrane permeability and facilitates virus release. EMBO J. **16:**3519–3532.
35. **Zazueta, C., M. E. Sosa-Torres, F. Correa, and A. Garza-Ortiz.** 1999. Inhibitory properties of ruthenium amine complexes on mitochondrial calcium uptake. J. Bioenerg Biomembr. **31:**551–557.